INTERNATIONAL JOURNAL FOR NUMERICAL METHODS IN FLUIDS, VOL. 14, 935–960 (1992)

AN EXTENSION OF OSHER'S RIEMANN SOLVER FOR CHEMICAL AND VIBRATIONAL NON-EQUILIBRIUM GAS FLOWS

R. ABGRALL, L. FEZOUI AND J. TALANDIER
INRIA, 2004 Route des Lucioles, Sophia Antipolis, F-06560 Valbonne, France

SUMMARY

In this paper we study an extension of Osher's Riemann solver to mixtures of perfect gases whose equation of state is of the form encountered in hypersonic applications. As classically, one needs to compute the Riemann invariants of the system to evaluate Osher's numerical flux. For the case of interest here it is impossible in general to derive simple enough expressions which can lead to an efficient calculation of fluxes. The key point here is the definition of approximate Riemann invariants to alleviate this difficulty.

Some of the properties of this new numerical flux are discussed. We give 1D and 2D applications to illustrate the robustness and capability of this new solver. We show by numerical examples that the main properties of Osher's solver are preserved; in particular, no entropy fix is needed even for hypersonic applications.

KEY WORDS Riemann solver Hypersonic flows

1. INTRODUCTION

During the past few years, because of the existence of many transatmospheric vehicle projects both in the U.S.A. and Europe, many researchers have been working on the numerical simulation of hypersonic flows.

Among the various methods proposed in the literature, upwind methods have encountered great success in the study of transonic and supersonic flows. A very natural wish is to extend them for hypersonic purposes. Besides the stiffness of the problem (very strong shock or expansion waves develop), new phenomena occur owing to the high level of temperature encountered in such gases; chemistry, vibrational relaxation and possibly ionization have to be taken into account. All classical Riemann solvers have been derived with the perfect gas law assumption and then have to be adapted to real gases.

Many solutions have been presented to generalize van Leer's solver[1–4] or Roe's solver[1,4–7] in thermal and chemical equilibrium. More recently, the same work has been done for non-equilibrium chemistry and non-equilibrium vibrational relaxation.[8–11]

In classical applications one of the most interesting solvers is that of Osher.[12] The principle of Osher's Riemann solver is to solve the Riemann problem by connecting the two states under consideration by three subpaths. Each of them consists of a compression or an expansion wave and a contact discontinuity, and then one has to average the flux on this multivalued path. We

0271–2091/92/080935–26$13.00
© 1992 by John Wiley & Sons, Ltd.
Received June 1990
Revised August 1991

will recall precisely how to build this numerical flux in Section 3.2. Two versions of Osher's solver are used depending on the path chosen in its definition.

The main properties of this numerical flux are (i) robustness, (ii) smoothness at transition points, (iii) satisfaction of an entropy inequality and (iv) stationary and sharp contact discontinuity and shocks. Property (iii) has been proved at least for one version of the scheme[12] but shown experimentally to be true for the other. This scheme uses information related to the Riemann problem. Its utilization for more general cases than that of perfect gases needs further work.

The extension of this particular Riemann solver was first (to our knowledge) generalized for real gases by Abgrall and Montagné,[13] then by Dubois[14] and very recently by Suresh and Liou.[15] The differences between these versions lie mainly in the method of calculating the ends of the connecting paths and the sonic points and how the true paths are approximated. The version presented by Abgrall and Montagné is simpler than that of Suresh and Liou and experimentally satisfies properties (i)–(iv), but the latter, depending on what computational effort is requested, may be more accurate and leads to variations. In Dubois' version one tries to tabulate the Riemann invariants of the problem.

In the present paper we adopt basically the same approach as that in Reference 13, i.e. we use approximate Riemann invariants since the exact ones are generally difficult to handle from a numerical point of view. Nevertheless, in this paper the expressions of approximate Riemann invariants that are derived are more closely related to the true ones. What are easy to get are differential equations satisfied by these Riemann invariants along paths colinear with the eigenvectors of the Jacobian matrix of the Euler flux terms.

From the expression of the Jacobian matrix we first study the behaviour of its eigenvalues. Then we describe the Riemann invariants of the system and propose and discuss a method for their integration.

Several test cases, both 1D and 2D are considered in order to study the efficiency and the robustness of the method. In particular, we compare our solver to the exact solution of a 1D shock tube problem with severe initial conditions.

2. EQUATION OF STATE, PHYSICAL MODEL, EIGENVALUES AND EIGENVECTORS

2.1. *Equation of state*

We consider a mixture of *ns* perfect gases. The internal energy of a given species is

$$\varepsilon_i = \rho_i c_{v_i} T + \rho_i h_i^0 + \rho_i e_{\text{vib}}^i,$$

where T is the translational temperature, h_i^0 is the enthalpy of formation of species i at a given reference temperature and e_{vib}^i is the specific vibrational of species i (this term disappears for the monoatomic species).

We assume that some of the diatomic species may not be at thermal equilibrium with the translational temperature T. Let T_i be the vibrational temperature of species i. We will assume that the vibrational energy E_{vib}^i is related to T_i and ρ_i by

$$E_{\text{vib}}^i = \rho_i \frac{\mathscr{R}_i \theta_i}{\exp(\theta_i/T_i) - 1} = \rho_i e_{\text{vib}}^i. \tag{1}$$

If species i is at thermal equilibrium, $T_i = T$ in equation (1).

The internal energy ε is the sum of each internal energy:

$$\varepsilon=\sum_{i=1}^{ns}\rho_i c_{v_i}T+\sum_{i=1}^{ns}\rho_i h_i^0+\sum_{i=1}^{nv_1}E_{\text{vib}}^i+\sum_{i=nv_1+1}^{nv}\rho_i e_{\text{vib}}^i. \tag{2}$$

In equation (2) nv is the number of diatomic species; they are assumed to be the nv first ones among which the nv_1 first diatomic species are not at thermal equilibrium. Thus in equation (2) $\varepsilon_{\text{vib}}^i$ is calculated with $T_i=T$ for $i=nv_1+1,\dots,nv$ and with a vibrational temperature different from T for the other terms $i=1,\dots,nv_1$.

The pressure is given by Dalton's law:

$$p=\sum_{i=1}^{ns}\rho_i c_{v_i}\kappa_i T=\rho c_v \kappa T, \tag{3}$$

where

$$c_v=\sum_{i=1}^{ns}Y_i c_{v_i},\qquad \kappa=\frac{\sum_{i=1}^{ns}Y_i c_{v_i}\kappa_i}{\sum_{i=1}^{ns}Y_i c_{v_i}}.$$

2.2. Euler equations

We consider thermal and vibrational non-equilibrium. The independent variables which describe the system are the partial densities, momentum ρu, total energy $e=\varepsilon+\frac{1}{2}\rho u^2$ and vibrational energies. In 1D they obey the Euler equation with possibly source terms if we consider chemistry and vibrational relaxation:

$$\frac{\partial W}{\partial t}+\frac{\partial F}{\partial x}=\Omega,$$

with

$$W=\begin{bmatrix}\rho_1\\ \vdots\\ \rho_{ns}\\ \rho u\\ e\\ E_{\text{vib}}^1\\ \vdots\\ E_{\text{vib}}^{nv_1}\end{bmatrix},\qquad F(W)=\begin{bmatrix}\rho_1 u\\ \vdots\\ \rho_{nv}u\\ \rho u^2+p\\ u(e+p)\\ E_{\text{vib}}^1 u\\ \vdots\\ E_{\text{vib}}^{nv_1}u\end{bmatrix},\qquad \Omega=\begin{bmatrix}\Omega_{\text{chim}}^1\\ \vdots\\ \Omega_{\text{chim}}^{ns}\\ 0\\ 0\\ \Omega_{\text{vib}}^1\\ \vdots\\ \Omega_{\text{vib}}^{nv_1}\end{bmatrix}. \tag{4}$$

In this paper our main objective is to derive an extension of Osher's Riemann solver for mixtures of perfect gases which may possibly include chemical and vibrational non-equilibrium phenomena. Thus we will concentrate on the discretization of the flux terms in equation (4); the precise expression of Ω is of no use now. It is given in Section 4.

2.2.1. Jacobian matrix. We immediately get

$$\frac{\partial F(W)}{\partial W}=\begin{bmatrix} (1-Y_1)u & \cdots & -Y_1u & Y_1 & 0 & 0 & \cdots & 0 \\ \vdots & \vdots & \vdots & \vdots & \vdots & \vdots & \vdots & \vdots \\ -Y_{ns}u & \cdots & (1-Y_{ns})u & Y_{ns} & 0 & 0 & \cdots & 0 \\ -u^2+p_{\rho_1} & \cdots & -u^2+p_{\rho_{ns}} & 2u+p_{\rho u} & p_E & p_{E^1_{\text{vib}}} & \cdots & p_{E^{nv_1}_{\text{vib}}} \\ (-H+p_{\rho_1})u & \cdots & (-H+p_{\rho_{ns}})u & H+p_{\rho u}u & (1+p_E)u & up_{E^1_{\text{vib}}} & \cdots & up_{E^{nv_1}_{\text{vib}}} \\ -uE^1_{\text{vib}}/\rho & \cdots & -uE^1_{\text{vib}}/\rho & E^1_{\text{vib}}/\rho & 0 & u & \cdots & 0 \\ \vdots & \vdots & \vdots & \vdots & \vdots & \vdots & \vdots & \vdots \\ -uE^{nv_1}_{\text{vib}}/\rho & \cdots & -uE^{nv_1}_{\text{vib}}/\rho & E^{nv_1}_{\text{vib}}/\rho & 0 & 0 & \cdots & u \end{bmatrix}, \tag{5}$$

where p_z stands for the partial derivative of p with respect to any conservative variable $z=\rho_i$ $(i=1,\ldots,ns)$, ρu, E, $E^i_{\text{vib}}(i=1,\ldots,nv_1)$. In equation (5) we have set

$$p_{\rho_i}=\chi_i+\kappa_{\text{so}}u^2/2, \qquad p_{\rho u}=-\kappa_{\text{so}}u, \qquad p_E=\kappa_{\text{so}}, \qquad p_{E^i_{\text{vib}}}=-\kappa_{\text{so}},$$

with

$$\kappa_{\text{so}}=\frac{\sum_{i=1}^{ns}Y_i\mathscr{R}_i}{\sum_{i=1}^{ns}Y_ic_{v_i}+\sum_{i=nv_1+1}^{nv}Y_i(\mathrm{d}e^i_{\text{vib}}/\mathrm{d}T)}, \qquad \chi_i=c_{v_i}(\kappa_i-\kappa_{\text{so}})T-\kappa_{\text{so}}(h_i^0+\sigma_ie^i_{\text{vib}}).$$

In the last expression $\sigma_i=1$ if species i is diatomic and at thermal equilibrium, $\sigma_i=0$ otherwise.

It is straightforward to check that the fluxes **F** are homogeneous of degree one and that the matrix $\partial F(W)/\partial W$ is diagonalizable and has real eigenvalues.

Right eigenvectors. The following matrix R describes its eigenvectors, the lth column of R being the lth eigenvector of $\partial F(W)/\partial W$:

$$R=\begin{bmatrix} 1 & 0 & \cdots & 0 & 0 & \cdots & 0 & Y_1 & Y_1 \\ 0 & 1 & \cdots & 0 & 0 & \cdots & 0 & Y_2 & Y_2 \\ \vdots & \vdots & \vdots & \vdots & \vdots & \vdots & \vdots & \vdots & \vdots \\ 0 & 0 & \cdots & 1 & 0 & \cdots & 0 & Y_{ns} & Y_{ns} \\ u & u & \cdots & u & 1 & \cdots & 1 & u-a & u+a \\ u^2/2-\chi_1/\tilde{\kappa} & u^2/2-\chi_2/\tilde{\kappa} & \cdots & u^2/2-\chi_{ns}/\tilde{\kappa} & 1 & \cdots & 1 & H-ua & H+ua \\ 0 & 0 & \cdots & 0 & 1 & \cdots & 0 & E^1_{\text{vib}}/\rho & E^1_{\text{vib}}/\rho \\ \vdots & \vdots & \vdots & \vdots & \vdots & \vdots & \vdots & \vdots & \vdots \\ 0 & 0 & \cdots & 0 & 0 & \cdots & 1 & E^{ns}_{\text{vib}}/\rho & E^{ns}_{\text{vib}}/\rho \end{bmatrix}.$$

In the matrix R the $ns+nv_1$ first columns are associated with the eigenvalue $\lambda_1=u$, the next column with $\lambda_2=u+a$ and the last column with $\lambda_3=u+a$, where a is the speed of sound, the square of which is

$$a^2=\sum_{i=1}^{ns}\chi_iY_i+\kappa_{\text{so}}\left(H-\sum_{nv_1+1}^{ns}e^i_{\text{vib}}-\frac{u^2}{2}\right). \tag{6}$$

Let us notice that the square of the speed of sound can also be written as

$$a^2=\gamma_{so}\frac{p}{\rho}, \tag{7}$$

with $\gamma_{so}=\kappa_{so}+1$. It is straightforward to check that the eigenvectors associated with λ_1 are linearly degenerate while those associated with the other eigenvalues are genuinely non-linear. More precisely, we have

(i) for $i=1,\ldots,ns+nv_1$, $\nabla\lambda_i\cdot R_i=0$
(ii) $\nabla(u-a)\cdot R_{ns+nv_1+1}=-(\gamma_{so}+1)a/2\rho<0$
(iii) $\nabla(u+a)\cdot R_{ns+nv_1+2}=(\gamma_{so}+1)a/2\rho>0$.

Left eigenvectors. One can easily get the left eigenvectors of the Jacobian matrix: they are linear forms whose expressions in term of any vector $V=(V_1,\ldots,V_{ns+nv_1+2})^T$ are

(i) for $i=1,\ldots,ns$,

$$l_i(V)=V_i-\frac{Y_i\kappa_{so}}{a^2}\left(V_{ns+2}-\sum_{l=ns+3}^{ns+nv_1+2}V_l-uV_{ns+1}+\frac{u^2}{2}\sum_{l=1}^{ns}V_l+\sum_{l=1}^{ns}\frac{\chi_l V_l}{\kappa_{so}}\right),$$

(ii) for $i=ns+1,\ldots,ns+1+nv_1$,

$$l_i(V)=V_i-\frac{E^i_{vib}}{\rho}\frac{\kappa_{so}}{a^2}\left(V_{ns+2}-\sum_{l=ns+3}^{ns+nv_1+2}V_l-uV_{ns+1}+\frac{u^2}{2}\sum_{l=1}^{ns}V_l+\sum_{l=1}^{ns}\frac{\chi_l V_l}{\kappa_{so}}\right),$$

(iii) for $i=ns+2+nv_1$, $ns+3+nv_1$,

$$l_i(V)=\frac{1}{2a}\left(V_{ns+1}-u\sum_{l=1}^{ns}V_l\right)\pm\frac{\kappa_{so}}{a^2}\left(V_{ns+2}-\sum_{l=ns+3}^{ns+nv_1+2}V_l-uV_{ns+1}+\frac{u^2}{2}\sum_{l=1}^{ns}V_l+\sum_{l=1}^{ns}\frac{\chi_l V_l}{\kappa_{so}}\right).$$

2.2.2. Riemann invariants. Here we intend to derive the differential equations satisfied by the Riemann invariants of the PDE system considered now without the source terms (i.e. $\Omega=0$):

$$\frac{\partial W}{\partial t}+\frac{\partial F(W)}{\partial x}=0,$$

where W and $F(W)$ have been defined in equations (4).

Let us consider an eigenvalue of $\partial F/\partial W$, say λ_k. A Riemann invariant associated with the eigenvalue λ_k is a function Φ^k of W such that for any eigenvector R_l which does not belong to the kernel of $\partial F/\partial W-\lambda_k Id$,

$$\nabla_W\Phi^k\cdot R_l=0.$$

The solutions of these sets of equations can be obtained in the phase space by considering the paths $s\mapsto W(s)$ such that dW/ds belongs to the eigenvector space associated with the eigenvalue k.

If we use the right eigenvectors defined above, we may see that the Riemann invariants, in the problem considered here, are solutions of the following differential equations.

(i) Eigenvalue $\lambda_1=u$:

$$\rho\frac{du}{ds}\pm\frac{1}{a}\frac{dp}{ds}=0. \tag{8}$$

(ii) Eigenvalue $\lambda_2 = u + a$:

$$\frac{d\rho_i}{ds} - \frac{Y_i}{a^2}\frac{dp}{ds}, \quad i = 1, \ldots, ns, \tag{9}$$

$$\frac{dY_i e^i_{vib}}{ds} - \frac{Y_i e^i_{vib}}{a^2}\frac{dp}{ds}, \quad i = 1, \ldots, nv_1, \tag{10}$$

$$\rho\frac{du}{ds} + \frac{1}{a}\frac{dp}{ds} = 0. \tag{11}$$

(iii) Eigenvalue $\lambda_3 = u - a$:

$$\frac{d\rho_i}{ds} - \frac{Y_i}{a^2}\frac{dp}{ds}, \quad i = 1, \ldots, ns, \tag{12}$$

$$\frac{dY_i e^i_{vib}}{ds} - \frac{Y_i e^i_{vib}}{a^2}\frac{dp}{ds}, \quad i = 1, \ldots, nv_1, \tag{13}$$

$$\rho\frac{du}{ds} - \frac{1}{a}\frac{dp}{ds} = 0. \tag{14}$$

We can see that there are two equations for λ_1 and $ns + nv_1 + 1$ equations each for λ_2 and λ_3.

Discussion. These differential equations may be difficult to solve (and in general impossible to solve by hand) because γ_{so} depends in general on both the temperature and the mass fraction. Nevertheless, it is possible to make some general comments.

1. Case of the linearly degenerate fields: it is obvious from equations (8) that the pressure p and the velocity u remain constant in a wave associated to λ_1.
2. Case of the genuinely non-linear fields: if one sums up equations (9), one gets

$$\frac{d\rho}{ds} = \frac{1}{a^2}\frac{dp}{ds}. \tag{15}$$

Since $Y_i = \rho_i/\rho$, we can deduce that the mass fractions Y_i remain constant in sonic waves. The same is true for the specific vibrational energy $E^i_{vib}/\rho = Y_i e^i_{vib}$.

The problem reduces to the integration of equations (15), (11) and (14). From the first we obtain the invariance of the specific entropy in expansion/compression waves:[16]

$$s = \sum_{i=1}^{ns} Y_i[c_{v_i}\log(p_i) - c_{p_i}\log(\rho)] + \sum_{i=nv_1+1}^{ns} Y_i\Phi_i(T), \tag{16}$$

where

$$\Phi_i(T) = \int_T \frac{d}{du} E^i_{vib}\frac{du}{u^2}$$

and

$$p_i = \rho_i\frac{\mathscr{R}}{m_i}T$$

is the partial pressure of species i. The integrals in equation (16) can be expressed by usual functions when one makes the harmonic oscillator assumption as we do in equation (1):

$$\Phi_i(T)=\mathscr{R}_i\theta_i\left\{\frac{\theta_i/T}{\exp(\theta_i/T)-1}+\frac{\theta_i}{T}-\log\left[\exp\left(\frac{\theta_i}{T}\right)-1\right]\right\}.$$

The integration of equations (11)–(14) leads to quadratures that are generally impossible. They give

$$u\pm\int_T\sqrt{\left(\frac{a}{\kappa_{so}T}\right)}\,\mathrm{d}T.$$

This last integral cannot be expressed by mean of classical functions even in the simplest case of the harmonic oscillator assumption, except in two cases: either $nv=0$ (i.e. no vibrational terms) or $nv=nv_1$.

For these reasons we will not try to use the true Riemann invariants in our derivation but will use approximate ones that will enable us to compute good approximations of the numerical dissipation involved in Osher's Riemann solver. This is explained in the following section.

3. AN EXTENSION OF OSHER'S RIEMANN SOLVER

This section is divided into three parts: first we recall the definition of Osher's Riemann solver in the most general case, then we present an approximation in the case we consider here and lastly we comment on some of its properties.

3.1. Definition of Osher's Riemann solver

We will recall some details of the Osher–Solomon[12] and Osher–Chakravarthy[17] solvers.

Let us take a hyperbolic partial differential system of equations in conservative form:

$$\frac{\partial W}{\partial t}+\frac{\partial F}{\partial x}(W)=0.$$

Osher's approximate Riemann solver is defined by

$$\mathscr{F}(U,V)=\tfrac{1}{2}\left(F(U)+F(V)-\int_\Gamma|A(W)|\,\mathrm{d}W\right),\tag{17}$$

where A is the Jacobian matrix of F, $|A|$ admits the same eigenvectors as A but its eigenvalues are the absolute values of those of A and the integral path Γ connects the two states U and V.

In References 12 and 17 the path Γ is always tangent to the right eigenspaces of matrix A and is the reunion of three subpaths, Γ_1, Γ_2 and Γ_3, where Γ_i is tangent to the eigenspace defined by λ_i. Different ways of ordering the eigenvalues of A can be considered. The optimum choices seem to be the 'natural' order $(u-a, u, u+a)$ or the 'reverse' order $(u+a, u, u-a)$. In Reference 12 it was shown that the definition of Osher's solver combined with the reverse order leads to a numerical flux which respects an entropy inequality for the semidiscrete scheme. To our knowledge, nothing has been done for the natural order.

In the following we use the reverse order, but all of what we say can easily be transposed to the other choice of parametrization.

3.2. *Expression of the numerical flux*

One introduces intermediate states which are the ends of paths Γ_1, Γ_2 and Γ_3. They are (see Figure 1)

$$U_{1/3}=\Gamma_2\cap\Gamma_1, \qquad U_{2/3}=\Gamma_3\cap\Gamma_1.$$

The definition of these intermediate states is made precise in Section 3.4. Since the eigenvectors associated with $u\pm a$ are genuinely non-linear, the eigenvalues $u\pm a$ may change their sign at most once. These points, if they exist, are called sonic points and are denoted by $\overline{U_{1/3}}$ and $\overline{U_{2/3}}$ in the paths Γ_2 and Γ_3 respectively.

(i) Case of the genuinely non-linear vectors:

$$\begin{aligned}\int_{\Gamma_1}|A|\,\mathrm{d}W&=\int_U^{\overline{U_{1/3}}}A^+\,\mathrm{d}W-\int_{\overline{U_{1/3}}}^{U_{1/3}}A^-\,\mathrm{d}W\\&=\operatorname{sign}[\lambda_1(U)]\,[F(\overline{U_{1/3}})-F(U)]\\&\quad+\operatorname{sign}[\lambda_1(\overline{U_{1/3}})]\,[F(U_{1/3})-F(\overline{U_{1/3}})].\end{aligned}\tag{18}$$

The same things can be done along path Γ_3.

(ii) Case of the linearly degenerate fields: we have shown in Section 2.2.2 that the velocity remains constant in a u-wave. Since the fluxes are homogeneous of degree one, we get

$$\int_{\Gamma_2}|A|\,\mathrm{d}W=\operatorname{sign}(U_{1/3})\,[F(U_{2/3})-F(U_{1/3})].\tag{19}$$

3.3. *Approximate Riemann invariants*

The paths are determined using the Riemann invariants since the invariants associated with a given wave remain, by definition, constant on that wave. In the perfect gas case, for example, it is very easy to determine exact formulae of the Riemann invariants, so the intermediate states are

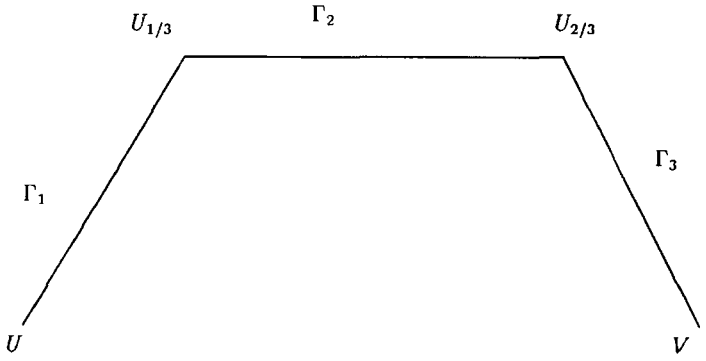

Figure 1. Paths and intermediate states

trivial to compute numerically. Here this is no longer true for the genuinely non-linear waves and the numerical solution to the equations which give the intermediate states would be very costly and practically unreachable in general. This is the reason why here we try to obtain approximate Riemann invariants which are as consistent as possible with the exact ones.

To begin with, let us recall the equations the invariants satisfy.

(i) The mass fractions Y_i and the specific vibrational energies E^i_{vib}/ρ for $i=1,\ldots,nv_1$ remain constant.

(ii) We have

$$\frac{d\rho}{ds}-\frac{1}{a^2}\frac{dp}{ds}=0, \tag{20}$$

$$\rho\frac{du}{ds}\pm\frac{1}{a}\frac{dp}{ds}=0. \tag{21}$$

On one hand, because of the expression of the speed of sound (6), equation (20) is equivalent to

$$dp=\left[\sum_{i=1}^{ns}\chi_i Y_i+\kappa_{so}\left(H-\sum_{1}^{nv_1}\frac{E^i_{\text{vib}}}{\rho}-\frac{u^2}{2}\right)\right]d\rho. \tag{22}$$

We also have, by definition

$$dp=\sum_{i=1}^{ns}\chi_i d\rho_i+\kappa_{so}d\varepsilon. \tag{23}$$

Since the mass fractions are constant, equations (21)–(23) lead to

$$\frac{d\varepsilon'}{\varepsilon'}=\left(1+\frac{p}{\varepsilon'}\right)\frac{d\rho}{\rho}. \tag{24}$$

In equation (24) we have set

$$\varepsilon'=\varepsilon-\sum_{i=1}^{nv_1}E^i_{\text{vib}}. \tag{25}$$

On the other hand, because of equation (7), equation (20) leads directly to

$$\frac{dp}{p}=\gamma_{so}\frac{d\rho}{\rho}. \tag{26}$$

To obtain easily the internal energy and the pressure from equations (24)–(26), one has to make two assumptions which we discuss below.

Assumption 1. $\gamma_{eq}=1+p/\varepsilon'$ is approximately constant in an expansion or a compression wave.
Assumption 2. The same is true for γ_{so}.

Discussion. These assumptions may not be justified from a pure mathematical point of view. Nevertheless, in our experience (shock tubes, blunt bodies and nozzles) they are not restrictive. Let us notice that γ_{eq} and γ_{so} are in general functions of the temperature T and the mass fractions. Since the mass fractions remain constant in an expansion/compression wave, both gammas depend only on the temperature. Moreover, if there are no vibrational terms (i.e. $nv=nv_1=0$) or if there are as many vibrational temperatures as diatomic species (i.e. $nv=nv_1$), then both gammas are equal and constant. In that case Assumptions 1 and 2 are no longer approximations.

In order to check the validity of our assumptions, the numerical experiments we have chosen here assume thermal equilibrium and begin with severe initial conditions. In that case the dependence of γ_{so} and γ_{eq} is not trivial and there is no particular relation between them, so Assumptions 1 and 2 may be very critical.

Derivation of the approximate Riemann invariants. If both assumptions are made the integration of equations (24) and (26) is trivial and leads to

$$\frac{\varepsilon}{\varepsilon_0}=\left(\frac{\rho}{\rho_0}\right)^{\gamma_{eq}}, \tag{27}$$

$$\frac{p}{p_0}=\left(\frac{\rho}{\rho_0}\right)^{\gamma_{so}}. \tag{28}$$

Equations (27) and (28) are approximations of the isentropic relation. They are obviously equivalent in the two extreme situations described above.

The integration of equation (21) is easy:

$$u\pm\frac{2}{\gamma_{so}-1}a=\text{constant}. \tag{29}$$

The approximate Riemann invariants are summarized in Table I.

3.4. *Determination of the intermediate states*

Here we show how to use these approximate Riemann invariants to get the intermediate states $U_{1/3}$ and $U_{2/3}$.

Table I

$u-a$	u	$u+a$
$\Psi_1^1=\dfrac{p}{\rho^{\gamma_{so}}}$ and $\Psi_1'^1=\dfrac{\varepsilon'}{\rho^{\gamma_{eq}}}$		$\Psi_{ns+nv_1+2}^1=\dfrac{p}{\rho^{\gamma_{so}}}$ and $\Psi_{ns+nv_1+2}'^1=\dfrac{\varepsilon'}{\rho^{\gamma_{eq}}}$
$\Psi_{i+1}^1=Y_i,\ i=1,\ldots,ns$	$\Psi_1^2=u$	$\Psi_{i+1}^{ns+nv+2}=Y_i,\ i=1,\ldots,ns$
$\Psi_{ns+i+1}^1=\dfrac{E_{\text{vib}}^i}{\rho},\quad i=1,\ldots,nv_1$		$\Psi_{ns+i+1}^{ns+nv+2}=\dfrac{E_{\text{vib}}^i}{\rho},\quad i=1,\ldots,nv_1$
$\Psi_{ns+nv_1+2}^1=u+\dfrac{2}{\gamma_{so}-1}a$	$\Psi_2^2=p$	$\Psi_{ns+nv_1+2}^{ns+nv_1}=u-\dfrac{2}{\gamma_{so}-1}a$

(i) For the wave associated with the eigenvalue $u-a$:

$$\left(\frac{p_L}{\rho_L}\right)^{\gamma_{so_L}}=\left(\frac{p_{1/3}}{\rho_{1/3}}\right)^{\gamma_{so_{1/3}}}, \qquad Y_i^L=Y_i^{1/3}, \quad i=1,\ldots,ns,$$

$$\frac{E^i_{vib_L}}{\rho_L}=\frac{E^i_{vib_{1/3}}}{\rho_{1/3}}, \quad i=1,\ldots,nv_1, \quad u_L+\frac{2}{\gamma_{so_L}-1}a_L=u_{1/3}+\frac{2}{\gamma_{so_L}-1}a_{1/3}.$$

(ii) For the wave associated with the eigenvalue $u+a$:

$$\left(\frac{p_R}{\rho_R}\right)^{\gamma_{so_R}}=\left(\frac{p_{2/3}}{\rho_{2/3}}\right)^{\gamma_{so_R}}, \quad Y_i^L=Y_i^{2/3}, \quad i=1,\ldots,ns,$$

$$\frac{E^i_{vib_R}}{\rho_R}=\frac{E^i_{vib_{2/3}}}{\rho_{2/3}}, \quad i=1,\ldots,nv_1, \quad u_R-\frac{2}{\gamma_{so_R}-1}a_R=u_{2/3}-\frac{2}{\gamma_{so_L}-1}a_{2/3}.$$

(iii) Through the contact discontinuity:

$$u_{1/3}=u_{2/3}, \qquad p_{1/3}=p_{2/3}.$$

Then, all the intermediates variables can be expressed by mean of the pressure $p=p_{1/3}=p_{2/3}$ and this leads to the equation

$$\frac{a_L}{\gamma_{so_L}-1}\left(\frac{p}{p_L}\right)^{(\gamma_{so_L}-1)/2\gamma_{so_L}}+\frac{a_R}{\gamma_{so_R}-1}\left(\frac{p}{p_R}\right)^{(\gamma_{so_R}-1)/2\gamma_{so_R}}=\tfrac{1}{2}(u_L-u_R)+\frac{a_L}{\gamma_{so_L}-1}+\frac{a_R}{\gamma_{so_L}-1}. \tag{30}$$

The non-linear equation is first preconditioned and the modified equation is solved by Newton iteration. Convergence is generally reached after two or three iterations. This technique has been developed in Reference 13 and is recalled later.

Once this is done, we have the values of the partial densities, velocity and pressure. We need the internal energy for computing the fluxes. This can be achieved by means of equation (27).

The sonic points, if they exist, are obtained with the approximate Riemann invariants as for the classical technique.

Remark. The internal energy and the pressure given by equations (27) and (28) are not generally consistent. The intermediate states $U_{1/3}$ and $U_{2/3}$ are 'pseudo'-intermediate states.

Discussion of equation (30). Equation (30) can be written as

$$f(p)=ap^\alpha+bp^\beta-c, \tag{31}$$

with suitable constants a, b, c, α and β. The function f is monotone-increasing, concave and equation (31) has an unique solution if and only if $c\geqslant 0$. Equation (31) could be solved by Newton iteration,

$$p_{n+1}=p_n-\frac{f(p_n)}{f'(p_n)},$$

but the method can lead to negative values of p if the initial guess p_0 is very large, because

$$\frac{f(p_n)}{f'(p_n)}\simeq\frac{p}{\max(\alpha,\beta)}.$$

The idea is to make a change of variable $z=x^{\xi}$, where $\xi=\max(\alpha, \beta)$, and to solve

$$g(z)=z+\frac{B}{A}z^{\eta}-\frac{c}{A}, \tag{32}$$

where

$$A=\tfrac{1}{2}[1-\operatorname{sign}(\alpha-\beta)]a+\tfrac{1}{2}[1+\operatorname{sign}(\beta-\alpha)]b,$$

$$B=\tfrac{1}{2}[1-\operatorname{sign}(\alpha-\beta)]b+\tfrac{1}{2}[1-\operatorname{sign}(\beta-\alpha)]a,$$

$$\eta=\frac{\min(\alpha, \beta)}{\max(\alpha, \beta)}\leq 1.$$

The function g is much easier to inverse than f: g is monotone-increasing, concave like f, but unlike f its derivative is *always* greater than unity. The convergence of the Newton iterations is guaranteed if the initial guess is less than the zero v of g.

One can localize v: it lies between the zeros of functions f_1 and f_2 which are defined by

$$f_1(p)=(a+b)p^{\alpha}-c, \qquad f_2(p)=(a+b)p^{\beta}-c.$$

We will usually start the Newton iteration with the smallest roots of f_1 and f_2. Convergence will usually be reached within two or three iterations.

3.5. A property of the numerical flux

In the kind of gas mixtures we study here we may have linear relations between the mass fractions of the various components. For the example of air these relations mean that the proportion of the number of moles of oxygen versus that of nitrogen is constant.

This can be formalized in the following way. We consider two linear forms $\Psi_1(W)=\sum_{i=1}^{ns} a_i\rho_i$ and $\Psi_2(W)=\sum_{i=1}^{ns} b_i\rho_i$. We assume that the admissible states lie in the affine space whose equation is

$$\alpha\Psi_1(W)=\beta\Psi_2(W), \tag{33}$$

where α and β are constant.

We now consider the first-order finite volume scheme whose numerical flux is that of Osher:

$$W_i^{n+1}=W_i^n-v_i(\mathscr{F}_{i+1/2}^n-\mathscr{F}_{i-1/2}^n). \tag{34}$$

In equation (34) v_i stands for the ratio of the time step and mesh size at node x_i. For the sake of clarity the integral part of Osher's flux will be denoted $d(W_i^n, W_{i+1}^n)$ or $d_{i+1/2}$.

We have to show that if relation (33) is true at iteration n, then it is true at iteration $n+1$. Since the forms Ψ_1 and Ψ_2 are linear and since we have

$$\Psi_1(F(W_i^n))=\Psi_2(W_i^n)u, \qquad \Psi_1(F(W_i^n))=\Psi_2(W_i^n)u,$$

where F is the continuous flux and u is the fluid velocity, we only have to show that

$$\alpha\Psi_1(d_{i+1/2}-d_{i-1/2})=\beta\Psi_2(d_{i+1/2}-d_{i-1/2}). \tag{35}$$

In Section 3.2 we have seen that the numerical dissipation $d(W_i^n, W_{i+1}^n)$ is a linear combination of the states W_i, W_{i+1}, the pseudostates $U_{1/3}$, $U_{2/3}$ and pseudosonic states. The coefficients in these linear combinations are independent of the partial densities. The partial densities of the pseudostates are

$$\rho_i^{1/3}=G_{\mathrm{L}}(p, \rho)\rho_{\mathrm{L}}, \qquad \rho_i^{2/3}=G_{\mathrm{R}}(p, \rho)\rho_{\mathrm{R}},$$

where the terms G_L and G_R do not depend on the partial densities. It is then obvious that for any l,

$$\alpha\Psi_1(d_{l+1/2}) = \beta\Psi_2(d_{l+1/2}).$$

This proves equation (35).

4. NUMERICAL EXPERIMENTS

This new solver have been tested on 1D and 2D cases. They are solved with the assumption of thermal equilibrium, which is the most unfavourable because of the assumptions we have made in Section 3.3; the values of γ_{so} and γ_{eq} which are used in the derivation of the approximate Riemann invariants depend explicitly on the vibrational energies of all diatomic molecules. If the approximations we make are not too well justified, we believe that we would not be able to run severe test cases, as we will show in this section. Calculations using different thermodynamics assumptions have also been done and are reported elsewhere.[18]

The scheme is based on a finite volume formulation. It is explicit for the convective terms and implicit for the source terms introduced by the dissociation–relaxation processes and the vibrational relaxation. The calculation uses the classical MUSCL method[19] in the 1D cases. The bidimensional calculations are done by using a finite element/finite volume/first-order approximation (see Reference 20 for details).

We have used the property of conservation of the proportion of species to reduce the size of the linear systems to solve at each time-step. For example, in 1D applications the original system is of size five. Since we have two linear combination of species, this implies the same relation for the source term. Thus the effective system to solve is only 3×3. The same idea is applied in the case of vibrational relaxation.

4.1. Chemical model

In the following we assume a mixture of the five main species which compose air: O, N, NO, O_2 and N_2; the relative proportion of oxygen versus that of nitrogen is 21/79. Vibrational equilibrium is assumed.

The dissociation and recombination model is that of Park,[21] in which we retain the 17 chemical reactions which involve O, N, NO, O_2 and N_2.

4.2. 1D test cases

We have run this new solver on numerous cases (e.g. those taken from Reference 22). We have chosen to report the results we have obtained on the one which seems to be the most difficult. It is taken from References 11 and 15 and is defined as follows:

(i) Left: $p = 100$ atm, $T = 9000$ K and $u = 0$.
(ii) Right: $p = 1$ atm, $T = 300$ K and $u = 0$.

This corresponds to the mass distribution given in Table II.

There is a large jump in pressure and temperature: the compositions of the mixture are completely different and so are the vibrational parts of the internal energy. This difficult test case has been chosen in order to test the assumptions made in Section 3.3. The calculations are of second-order spatial accuracy and use the limitation procedure on the characteristic variables.

Frozen case. As a first experience we intend to test this solver without any chemistry source terms. The calculations have been performed with a CFL number of 0·95 and use 101 points. The

Table II

T	ρ	Y_O	Y_N	Y_{NO}	Y_{O_2}	Y_{N_2}
9000	2·532	0·220	0·314	$2·3 \times 10^{-2}$	$7·36 \times 10^{-4}$	0·442
300	1·156	0	0	0	0·233	0·767

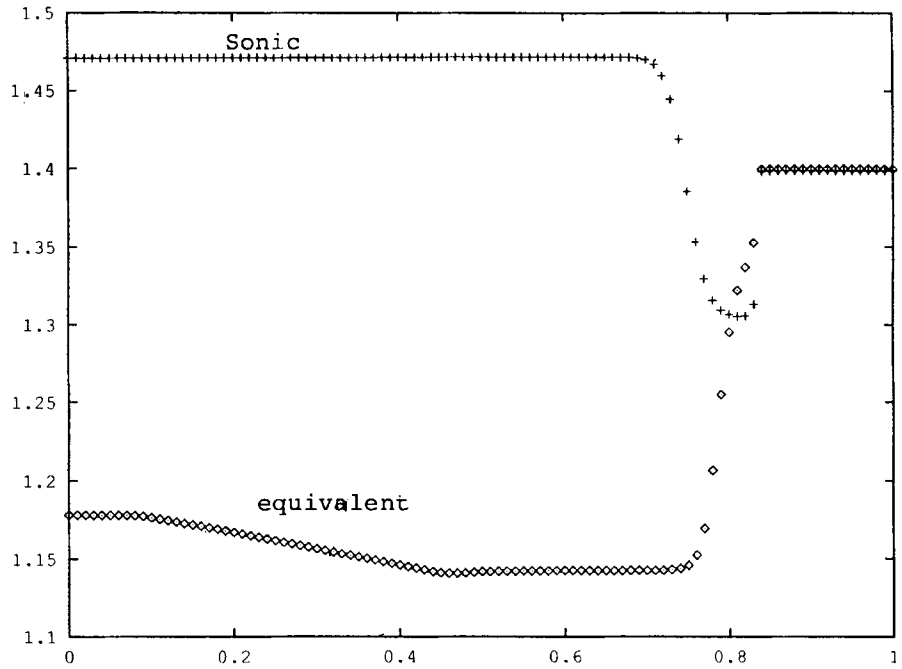

Figure 2. Equivalent and sonic gamma, frozen case

results are compared with the exact solution obtained by Colella and Glaz's method[23] adapted to the present situation. One can see that, despite the resolution, the agreement is excellent.

In Figure 2 we have plotted the two gammas which are used in the computation of the intermediate states. If non-equilibrium vibrational effects were present, the two gammas would be equal and the approximate Osher solver would be an exact one. We can see that their behaviour is different: the sonic gamma is constant in the expansion wave while the equivalent gamma $(1+p/\varepsilon')$ is not.

In Figure 3 one can see the mass fraction distributions. They are constant except at the contact discontinuity ($x \simeq 0·75$), as should be the case.

In Figures 4–8, where we have displayed the Mach number, pressure, density, temperature and velocity, we can see a small overshoot (or undershoot) at the end of the expansion wave. Even in the perfect gas case one can see this default because of the strength of the expansion wave. We insist that it is neither a consequence of the approximation we have made here nor a consequence of the second-order extension of the scheme.

The pressure and velocity remain constant at the contact discontinuity (Figures 4 and 5).

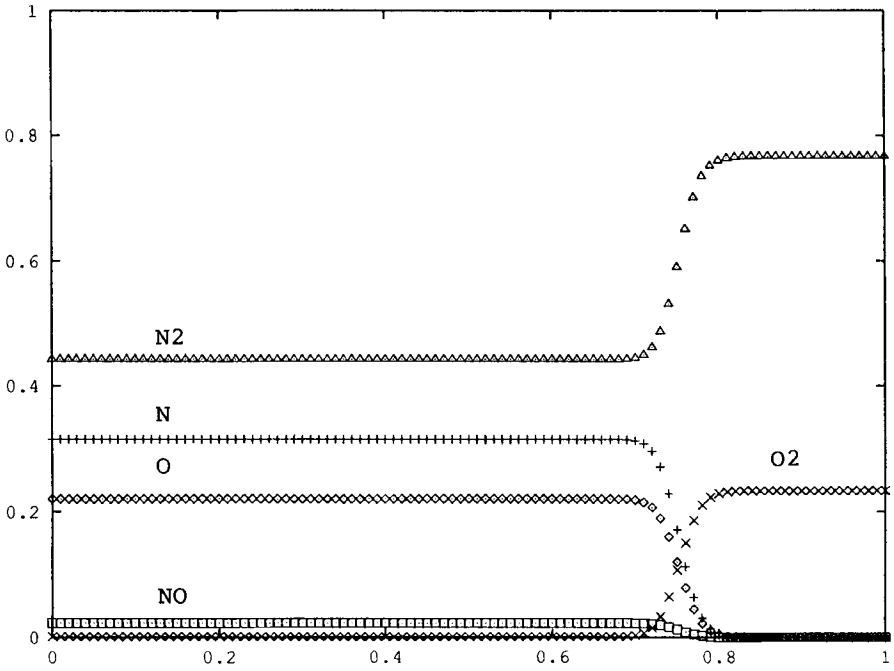

Figure 3. Mass fraction distribution, frozen case

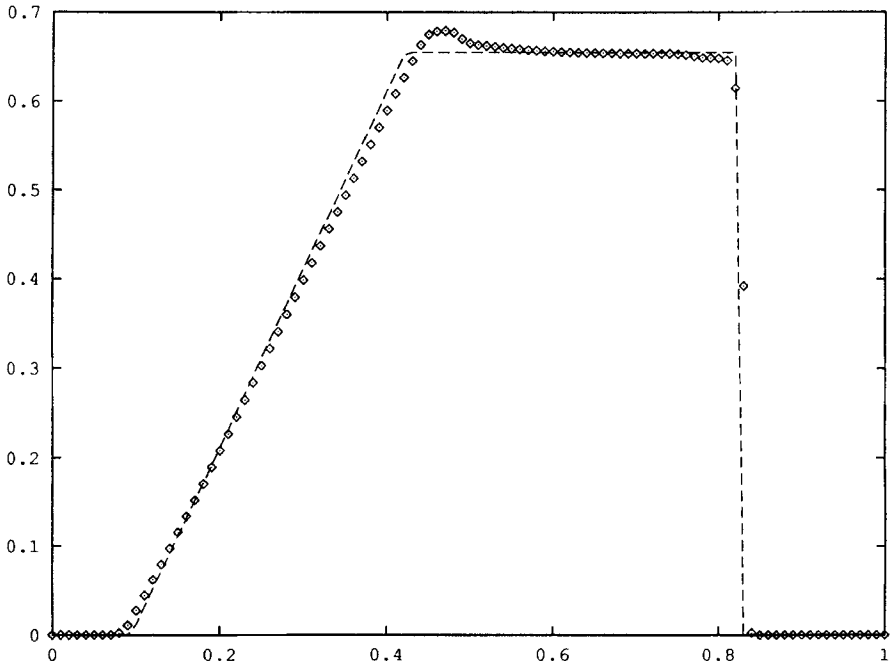

Figure 4. Velocity, Frozen case, --- exact, ◇ ◇ present solver

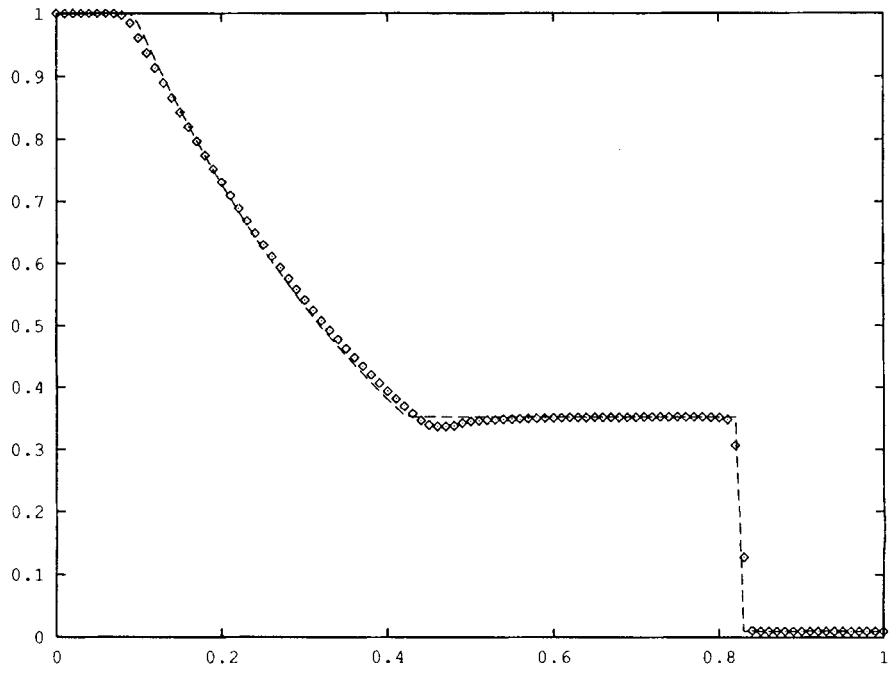

Figure 5. Pressure, Frozen case, --- exact, ◇ ◇ present solver

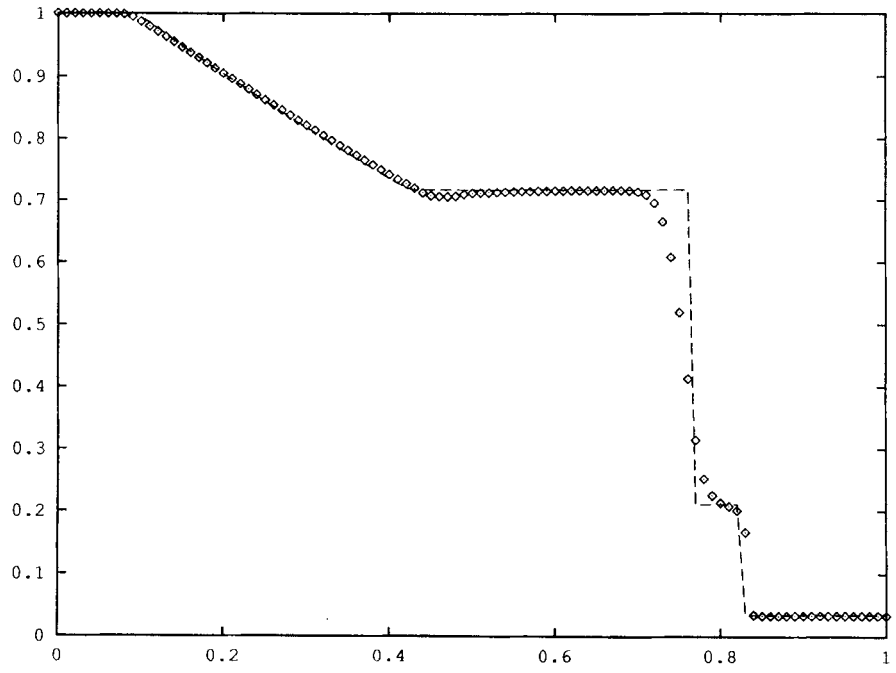

Figure 6. Temperature, frozen case, --- exact, ◇ ◇ present solver

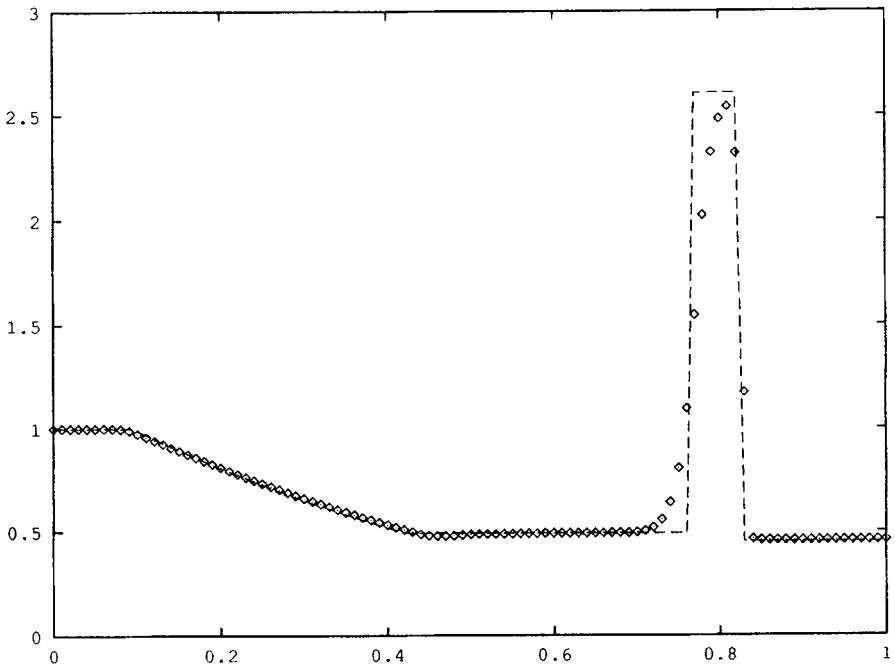

Figure 7. Density, frozen case, – – – exact, ◇ ◇ present solver

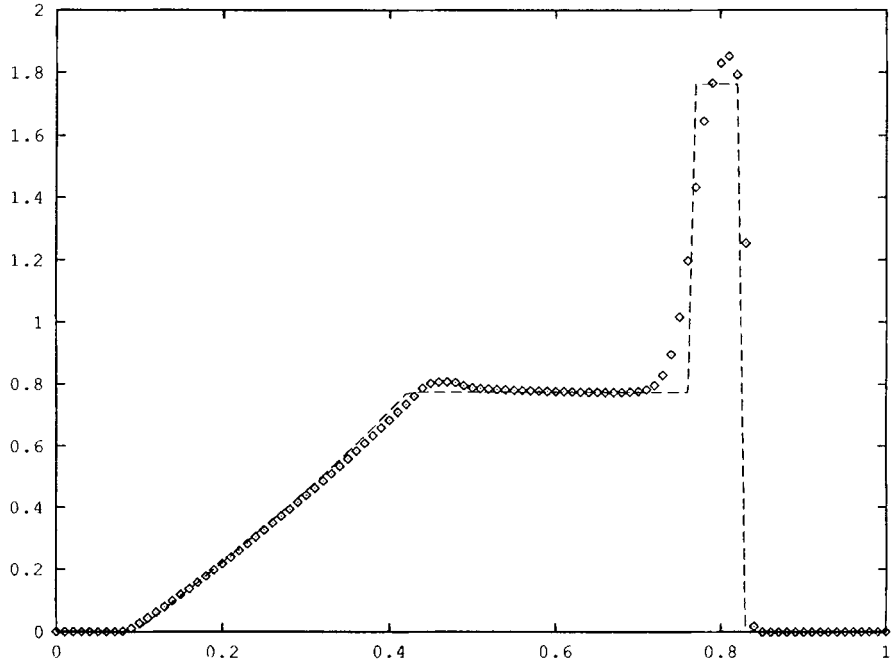

Figure 8. Mach number, frozen case, – – – exact, ◇ ◇ present solver

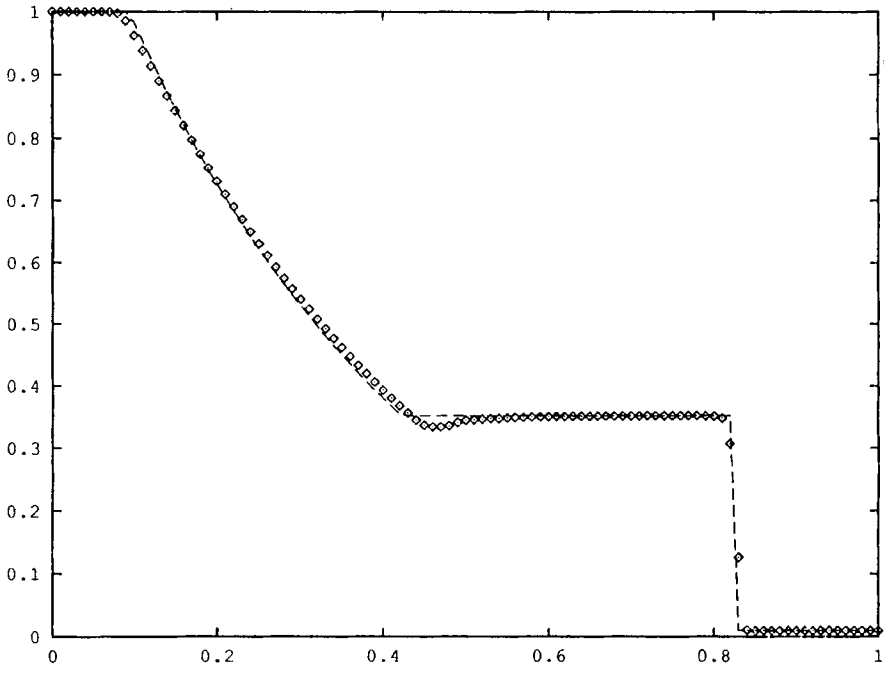

Figure 9. Pressure, frozen case, – – – exact, ◇ ◇ Roe's solver

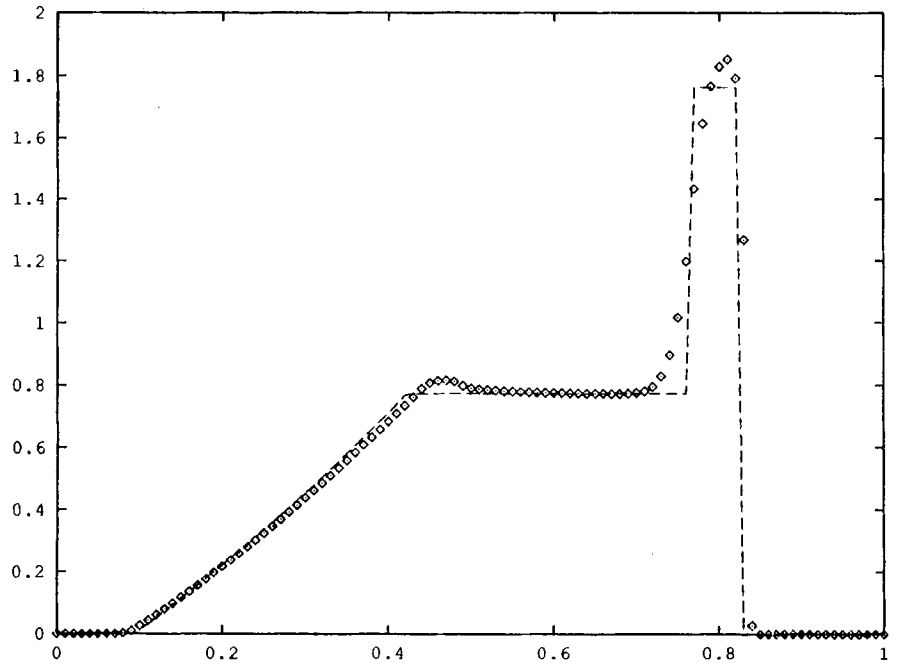

Figure 10. Mach number, frozen case, – – – exact, ◇ ◇ Roe's solver

Comparison with an extension of Roe's Riemann solver. The Mach number and pressure are given in Figures 9 and 10. These results are obtained by the same scheme with the extension of Roe's Riemann solver derived for thermal equilibrium flows[6] instead of the present version of Osher's solver. As we can see, the results are nearly the same. However, we must notice that the Roe calculations need an entropy fix.[24] If this correction is not used, the computation diverges irrespective of the CFL number. This demonstrates the robustness of the algorithm.

Test with chemistry source terms. In Figures 11–17 we have plotted the same variables as previously but with Park's model as chemistry source term. As we can see, the addition of chemical source terms does not alter the quality of the results. The methodology can easily handle more complicated situations. Here the calculations use 201 grid points in order to compare with References 11 and 15. The agreement with the former reference is good.

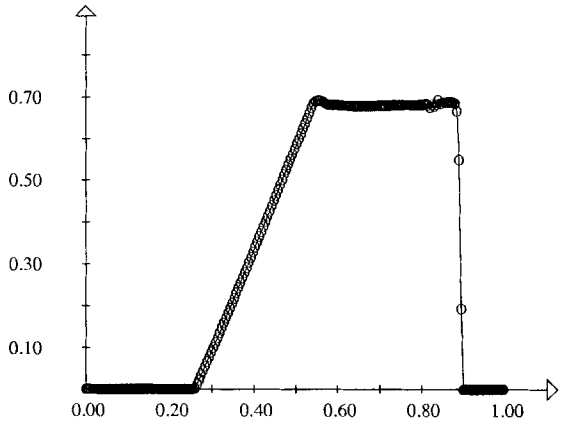

Figure 11. Velocity, non-equilibrium case

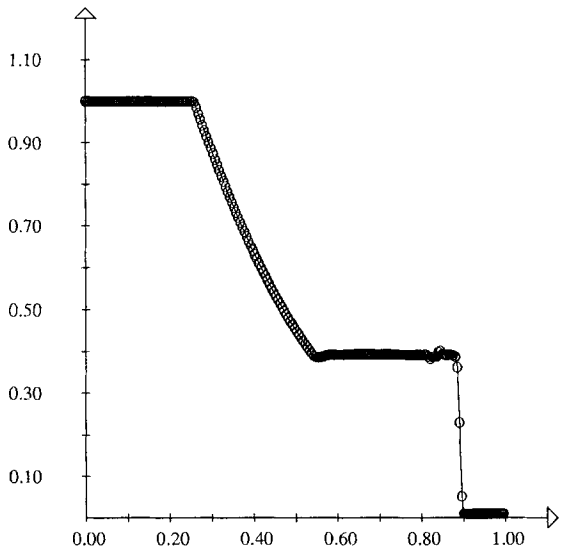

Figure 12. Pressure, non-equilibrium case

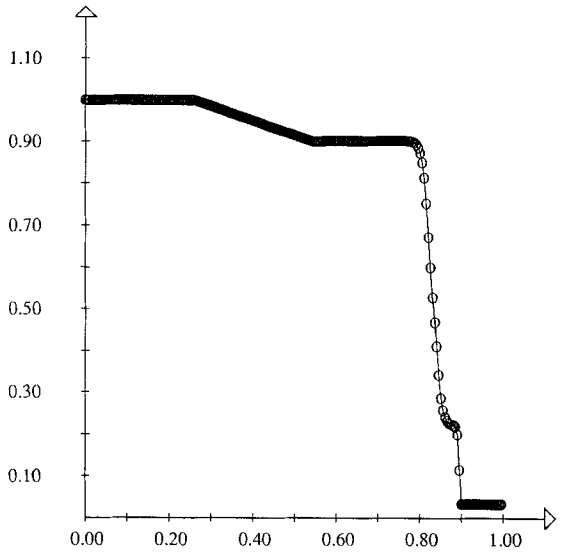

Figure 13. Temperature, non-equilibrium case

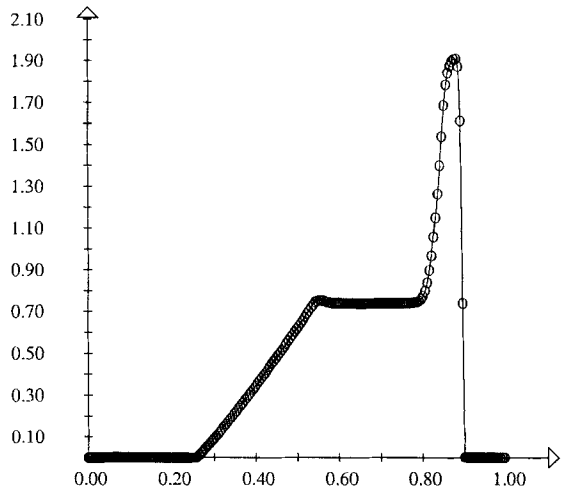

Figure 14. Mach number, non-equilibrium case

On the mass fraction (Figure 15) and temperature (Figure 13) plots we can see the differences between the non-chemistry calculations and this one. We notice a production of NO at the contact discontinuity. This explains the small wiggles in the velocity (Figure 11) and pressure (Figure 12) at this location: the ratios of specific heats of different species are different (1·4 or 1·66); at the contact discontinuity the dominant species are N_2, O, O_2 and NO. Since the numerical thickness of this discontinuity is not zero, this induces wiggles on the pressure and then on the velocity. This phenomenon would also be present if we had an exact solver at our disposal.[25,26]

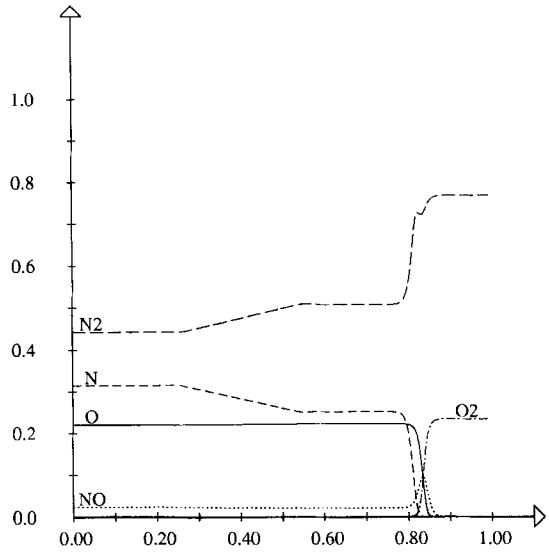

Figure 15. Mass fraction distribution, non-equilibrium case

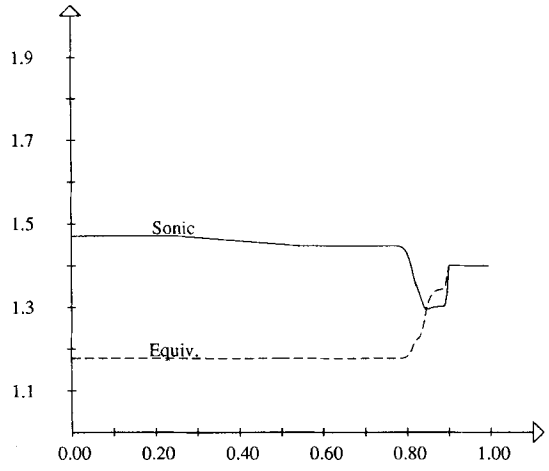

Figure 16. Equivalent and sonic gamma, non-equilibrium case

4.3. 2D test case

We have tested our solver on a test case defined for the Workshop on Hypersonic Flows for Reentry Problems held in Antibes, France in January 1990.[27]

The calculation is done on a double ellipse with a semi-axis of 60 cm. The conditions are defined at 75 km height and are

(i) pressure $P = 2{\cdot}52$ Pa
(ii) temperature $T = 204{\cdot}3$ K
(iii) density $0{\cdot}4276 \times 10^{-4}$ kg m^{-3}.

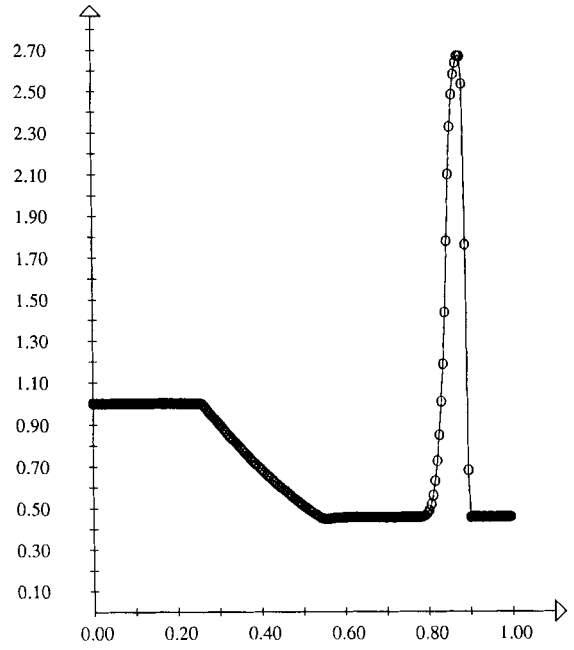

Figure 17. Density, non-equilibrium case

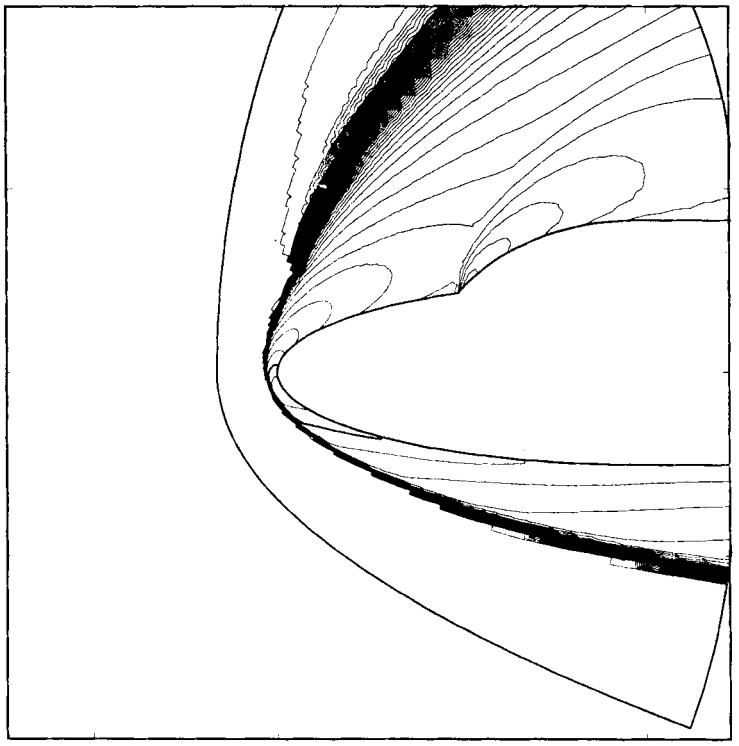

Figure 18. Iso-Mach lines, min = 0, max = 25, dM = 0·25

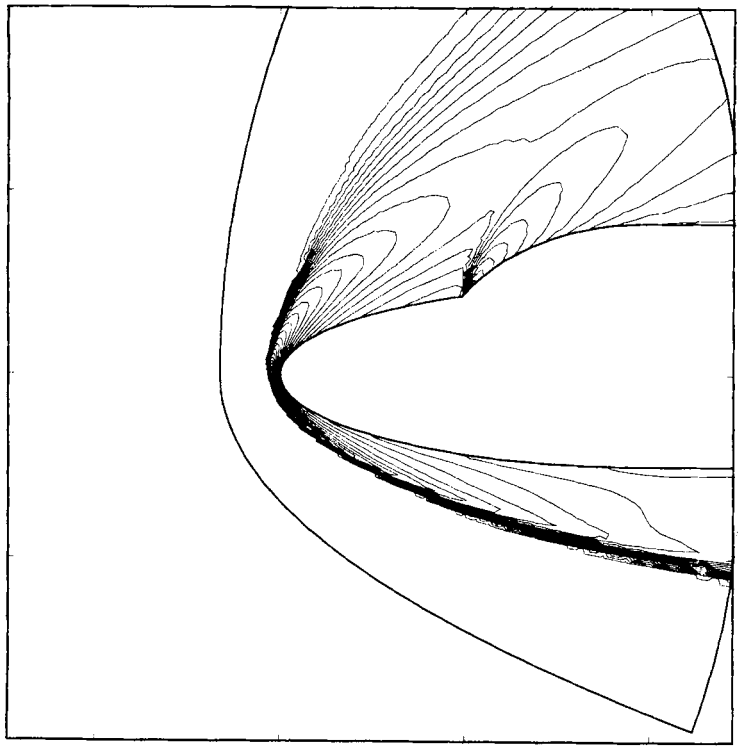

Figure 19. Temperature lines, min = 203 K, max = 15929 K dT = 500 K

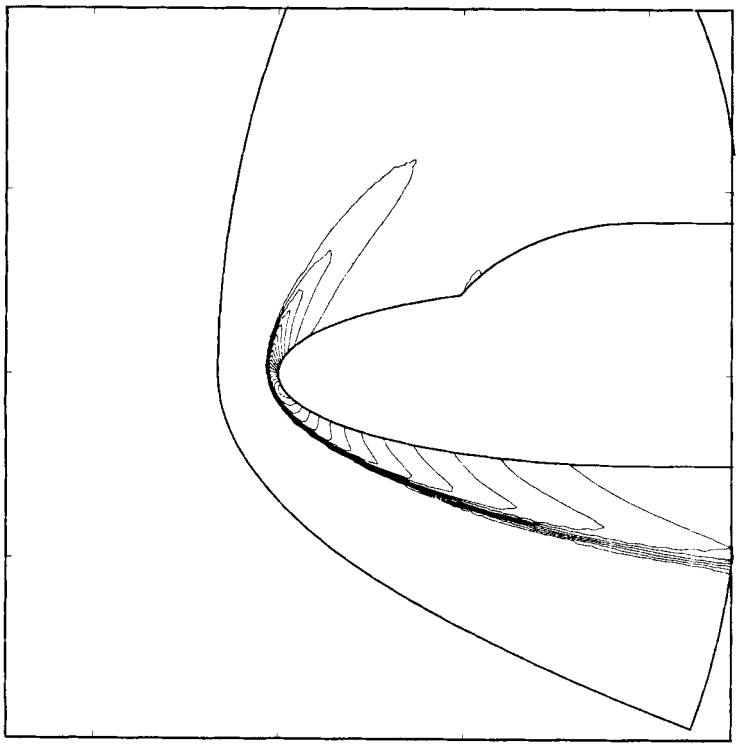

Figure 20. Pressure coefficient, min = −1·88, max = 0 dC_p = 0·1

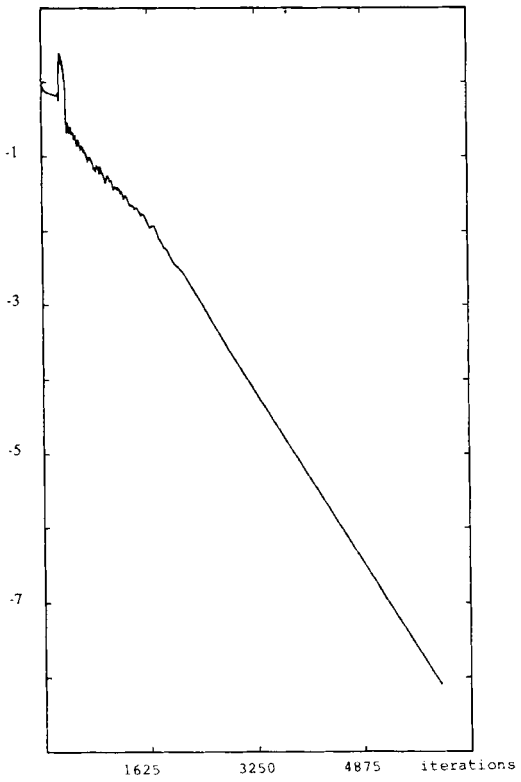

Figure 21. Convergence history, $\log_{10}$ of L^2 norm of the density

We assume thermal equilibrium. The calculation is done at $\mathcal{M}_\infty = 25$ and the angle of incidence is 30°. Some results are displayed in Figures 18–21. They include Mach number, temperature and pressure coefficient lines. The results compare very well with those obtained, for example, by Botta *et al.*[28] The convergence history of the calculation is given in Figure 21. From it, one can see that the convergence is very smooth. No particular trick has been used: the initial state is the uniform field at infinity and the computation was driven directly without gradually increasing the angle of incidence form 0° to 30°. At the beginning of the run the CFL number is set equal to 0·5 until the very-low-pressure areas just in front of the canopy and above the shuttle, caused by the severe initialization conditions we have taken, have disappeared; then the CFL number is set to 0·8.

5. CONCLUSIONS

We have presented here an extension of Osher's Riemann solver. The numerical tests we have performed show the robustness of this new solver. They also show that the properties of the Osher splitting (smoothness and physical shocks) are valid despite the assumptions we have made. In particular, no entropy fix is needed to capture shocks. The same techniques can also be used for more complex situations, e.g. ionized gas flows.

In conclusion, this extension gives satisfactory results in the applications. The accuracy of the spatial approximation may be extended to second-order in the 2D case. The convergence to

steady state may be accelerated by using an implicit δ-scheme for example. These two points are currently under study.

ACKNOWLEDGEMENTS

We wish to thank our collegue J. A. Désideri for providing us with the mesh used in Section 4.3, J. M. Roquejoffre of Centre de Mathématiques Appliquées de l'Ecole Polytechnique (France) for helping us to obtain the exact solution of the frozen Riemann problem as well as the anonymous referees whose comments have led to drastic improvements in this paper.

APPENDIX: NOTATIONS

$\mathscr{R}$	universal constant of perfect gases
m_i	molar weight of species i
$\mathscr{R}_i$	$\mathscr{R}/m_i$
c_{v_i}, c_{p_i}	specific heats of species i
γ_i	c_{p_i}/c_{v_i}
κ_i	$\gamma_i - 1$
T	temperature of flow
ρ_i	density of species i
ρ	total density, $\rho = \sum_{i=1}^{ns} \rho_i$
Y_i	mass fraction of species i, $Y_i = \rho_i/\rho$
h_i^0	enthalpy of formation of species i
θ_i	typical value of vibrational temperature of molecules of species i
p	pressure
u	velocity
m	momentum, $m = \rho u$
e	total energy per unit volume
ε	specific energy per unit mass
e^i_{vib}	specific vibrational energy of species i
E^i_{vib}	vibrational energy of species i, $E^i_{\text{vib}} = \rho_i e^i_{\text{vib}}$
H	specific enthalpy, $H = (e+p)/\rho$

REFERENCES

1. B. Grossman and R. W. Walters, 'An analysis of flux-split algorithms for Euler's equation real gases', *8th Computational Fluid Dynamics Conf.*, AIAA, New York, 1987, p. 177.
2. M. Vinokur and J. L. Montagne, 'Generalized flux-vector splitting for an equilibrium real gas', *Tech. Rep. 177513*, NASA, December 1988.
3. J. L. Montagné, 'Recherche fondementales sur les méthodes numériques pour les écoulements hypersoniques', *Tech. Rep. 16/1123 AY 218A*, ONERA, January 1988.
4. M. S. Liou, B. van Leer and J. S. Shuen, 'Splitting of inviscid fluxes for real gases', *J. Comput. Phys.*, **87**, 1–24 (1990).
5. M. Vinokur, 'Flux Jacobian matrices and generalized Roe average for an equilibrium real gas', *Tech. Rep. 177512*, NASA, December 1988.
6. R. Abgrall, 'An extension of Roe's upwind scheme to algebraic equilibrium real gas models', *Tech. Rep. 1189*, INRIA, March 1990.
7. P. Glaister, 'An approximate linearised Riemann solver for the Euler equations for real gases', *J. Comput. Phys.*, **74**, (1988).
8. R. Abgrall, 'Preliminary results on the extension of Roe's Riemann solver to non-equilibrium flows', *Tech. Rep. 987*, INRIA, March 1989.
9. B. Grossman and P. Cinnella, 'Flux-split algorithms for flows with non-equilibrium chemistry and vibrational relaxation', *Tech. Rep. 88-08-03*, ICAM, 1988.

10. Yen Liu and M. Vinokur, 'Nonequilibrium flows computations: I. An analysis of numerical formulations of conservation laws', *Tech. Rep. 177489*, NASA, 1989.
11. J. S. Shuen, B. van Leer and M. S. Liou, 'A detailed analysis of inviscid flux splitting algorithms for real gases with equilibrium of finite-rate chemistry', *Int. Conf. on Numerical Methods*, Williamsburg, VA, June 1988.
12. F. Solomon and S. Osher, 'Upwind difference scheme for hyperbolic systems of conservation laws', *Math. Comput.*, **38,** 339–374 (1982).
13. R. Abgrall and J. L. Montagné. 'Extension of Osher's Riemann solver for mixtures of perfect gases and real gases', *Rech. Aérospatiale*, **4**(4), 1–13 (1989).
14. F. Dubois, 'Programm TEBALDI—evaluation du flux d'Osher pour l'air à l'équilibre chimique', *Tech. Rep. 104/88*, Aérospatiale, April 1989.
15. A. Suresh and M. Liou, 'The Osher scheme for real gases', *AIAA Paper 90-0397*, 1990.
16. A. Decamps, Private communication, 1990.
17. S. Osher and S. Chakravarthy, 'Numerical experiments with the Osher upwind scheme for the Euler equations', *AIAA J.*, **21** (1983).
18. R. Abgrall, 'Hypersonic calculations by Riemann solver techniques', in K. Gustafson (ed.), *Computer Physics Communications*, Elsevier, Amsterdam, vol. 65, 1991, pp. 1–7.
19. B. van Leer, 'Towards the ultimate conservative difference scheme, III', *J. Comput. Phys.*, **23,** 263–275 (1977).
20. L. Fezoui and B. Stoufflet, 'A class of implicit upwind schemes for Euler simulations with unstructured meshes', *J. Comput. Phys.*, **84,** 174–206 (1989).
21. C. Park, 'On the convergence of chemically reacting flows', *AIAA Paper 85-0247*, 1985.
22. H. C. Yee, M. Vinokur and J. L. Montagné, 'Comparative study of high-resolution shock-capturing schemes for real gas', *Tech. Rep. TM-86839*, NASA, July 1987.
23. P. Colella and H. M. Glaz, 'Efficient solution algorithms for the Riemann problem for real gases', *J. Comput. Phys.*, **59,** 264–289 (1985).
24. A. Harten and J. Hyman, 'A Self-adjusting grid for the computation of weak solutions of hyperbolic conservation laws', *Rep. LA9105*, Center for Nonlinear Studies, Theoretical Division, Los Alamos National Laboratory, 1981.
25. R. Abgrall, 'Generalization of Roe's Riemann solver to mixture of perfect gas', *Rech. Aérospatiale*, **4,** 1–13 (1988).
26. B. Larrouturou and L. Fezoui, 'On the equation of multi-component perfect or real gas inviscid flow', Non linear hyperbolic problems, Lecture notes in Mathematics, Vol. 1402, pp. 69–98, Carasso, Charrier, Hanouzet and Joly (eds), Springer Verlag, Heidelberg (1989).
27. *Hypersonic Flows for Reentry Problems, Part I*, Proceedings of a workshop held in Antibes (France), 22–25 January 1990, Desideri, Glownisky and Périaux (eds), Springer Verlag 1991.
28. N. Botta, M. C. Ciccoli, J. A. Desideri, L. Fezoui, N. Glinsky, E. Hettena and C. Olivier, 'Reactive flows over the double ellipse', *Workshop on Hypersonic Flows for Reentry Problems*, INRIA–GAMNI, December 1988, Contribution 36.